World Electric Vehicle Journal

MDPI

Article

Improvement of the Vehicle Seat Suspension System Incorporating the Mechatronic Inerter Element

Chengqun Qiu [1,*], Xiaofu Liu [2] and Yujie Shen [3]

[1] Jiangsu Province Intelligent Optoelectronic Devices and Measurement-Control Engineering Research Center, Yancheng Teachers University, Yancheng 224007, China
[2] College of Engineering, China Agricultural University, Beijing 100083, China
[3] Automotive Engineering Research Institute, Jiangsu University, Zhenjiang 212013, China
* Correspondence: yctcqcq@126.com; Tel.: +86-15805108661

Abstract: A mechatronic inerter can simulate the equivalent mechanical network through the external electrical network and can be used in a wide range of mechanical device design applications. In this paper, we study the use of a mechatronic inerter to enhance vibration isolation in vehicle seat suspensions. Firstly, the vertical and pitch movements of the vehicle's sprung mass and the vertical vibration of the seat are considered in a half vehicle model. Then, the mechatronic inerter is introduced and the external electrical network is presented. The particle swarm optimization algorithm was used to optimize the seat suspension layout parameters with different transfer function-orders. Numerical simulations under different speeds were performed, and the results show that the application of the used mechatronic inerter's seat suspension vibration isolation performance outperforms passive suspension. In addition, with an increase in the external electrical network transfer function-order, the seat acceleration and pitch acceleration RMS values will be further reduced. The results of the study will contribute to a new approach to vehicle seat suspension design.

Keywords: vehicle; seat suspension; inerter; mechatronic system

Citation: Qiu, C.; Liu, X.; Shen, Y. Improvement of the Vehicle Seat Suspension System Incorporating the Mechatronic Inerter Element. *World Electr. Veh. J.* **2023**, *14*, 29. https://doi.org/10.3390/wevj14020029

Academic Editors: Yong Li, Xing Xu, Lin Zhang, Yechen Qin and Yang Lu

Received: 12 December 2022
Revised: 15 January 2023
Accepted: 18 January 2023
Published: 23 January 2023

1. Introduction

Seat suspension is used in vehicles in order to enhance the driver's comfort and protect the health of the driver from vibrations caused by uneven roads. Improved driver ride comfort can be achieved by designing the ride quality of the main and cockpit suspensions [1–4]. However, for commercial vehicles, the driver is primarily exposed to high amplitude and low frequency vibrations, which are a major factor in health disorders [5,6]. Therefore, using the seat's suspension to reduce unwanted vibration is a simple and effective method. In particular, Deng proposed, in 2019, a novel seat suspension capable of variable stiffness and damping (VSVD) that improved ride comfort with magnetorheological fluid dampers [7]. In [8], Ning proposed an electrical variable stiffness device (EVSD) and applied it to suspensions in 2019. The introduction of a negative stiffness structure into a cab seat suspension structure improved the cab's working environment and the seating comfort in [9]. In [10], Liu proposed a semi-active electromagnetic device capable of varying inertance and damping (VIVD), using an energy storage priority control (ESPC) strategy to reduce the vibrations in vehicle seat suspensions in 2021. Until now, several scholars have proposed a number of different structures for seat suspension, and the structural aspect of improving the performance of seat suspension has reached a bottleneck. The question of how to design a new seat suspension structure with excellent performance has becomes a heated problem.

Inerters, such as springs and dampers, are strictly mechanical components with two endpoints [11–13]; the use of such results in significant improvements in vehicle suspension system performance [14,15]. Professor Smith gave the physical definition and dynamic equations of the inerter device, and designed the rack-pinion inerter and ball-screw inerter. The application of an inerter element was further studied in a vehicle suspension system [16–18] and in civil engineering [19,20]. In [21], Liu proposed a new semi-active suspension system based on a hydro-pneumatic inerter, and an MPC control strategy was designed to suppress vehicle vibration in 2021. In [22], use of electrical network elements for equivalent fractional-order mechanical networks in vehicle suspension design showed that the results of numerical simulations confirm the performance advantages of vehicle mechatronic ISD suspension with a fractional-order electrical network. In [23], Li effectively used the advantages of an inertial suspension and GH control strategy to reduce dynamic tire loads in HMDVs over a wider frequency range in 2022. In [24–26], the effect of inerter nonlinearity on vehicle suspension vibration isolation performance was studied. In [27], inerter development led to a new theory of electromechanical similarity, where an inerter corresponds to a capacitor, a damper corresponds to a resistor, and a spring corresponds to an inductor. Shen proposed an optimal design method for vehicle mechatronic ISD suspension based on the structure-immittance approach in 2021 [28]. However, the application of an inerter element to a vehicle seat suspension system lacks research. Based on the new electromechanical similarity theory, the ability to use an external electrical network can increase the order of the seat suspension's transfer function and simplify the mechanic. Therefore, in order to improve vibration isolation performance and the ride comfort of seat suspension, this paper integrates a mechatronic inerter element into vehicle seat suspension. The article is structured as follows.

Firstly, in Section 2, a half vehicle model is established with a seven-degree-of-freedom model that takes into account the vertical and pitch movements of the vehicle's sprung mass and the vertical vibration of the seat. Then, in Section 3, the seat suspension, employing a mechatronic inerter device, is introduced, and the different external electrical networks are presented. In Section 4, the particle swarm optimization algorithm is used to optimize the designed seat suspension parameters. Then, Section 5 provides an analysis of the seat suspension dynamics according to the half vehicle model. Section 6 is the concluding section of this paper.

2. Half Vehicle Model

We refer to the half vehicle model built by Shen in 2021 [28]. Figure 1 shows the half vehicle model built for this study; this seven-degree-of-freedom model takes into account the vertical and pitch movements of the vehicle's sprung mass and the vertical vibration of the seat. This study was carried out with the vehicle unloaded, therefore, the mass and inertia of the driver are not taken into account.

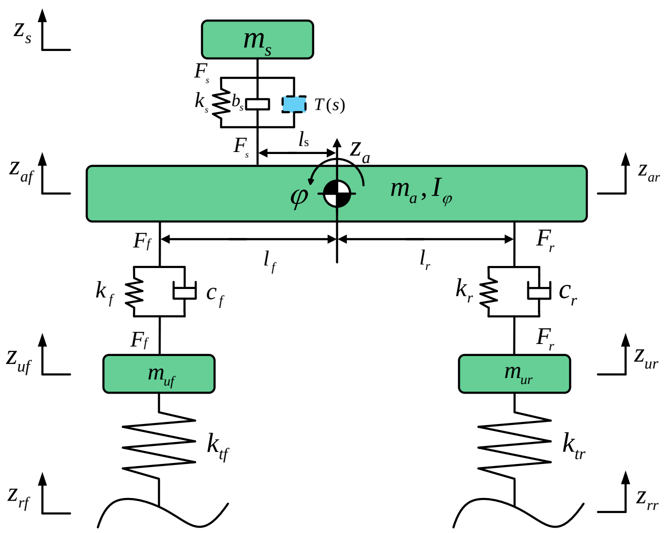

Figure 1. Seven-degree-of-freedom vehicle model.

The vertical motion equation of the seat mass is

$$m_s \ddot{z}_s = F_s \tag{1}$$

The equation representing the sprung mass vertical motion is

$$m_a \ddot{z}_a = k_f(z_{uf} - z_{af}) + c_f(\dot{z}_{uf} - \dot{z}_{af}) + k_r(z_{ur} - z_{ar}) + c_r(\dot{z}_{ur} - \dot{z}_{ar}) - F_s \tag{2}$$

The equation representing the sprung mass pitch motion is

$$I_\varphi \ddot{\varphi} = l_r F_r + l_s F_s - l_f F_f \tag{3}$$

The equations of the front and rear unsprung masses are

$$\begin{cases} m_{uf}\ddot{z}_{uf} = k_{tf}(z_{rf} - z_{uf}) - k_f(z_{uf} - z_{af}) - c_f(\dot{z}_{uf} - \dot{z}_{af}) \\ m_{ur}\ddot{z}_{ur} = k_{tr}(z_{rr} - z_{ur}) - k_r(z_{ur} - z_{ar}) - c_r(\dot{z}_{ur} - \dot{z}_{ar}) \end{cases} \tag{4}$$

The pitch angle can be approximately equal to the following equation when the angle is relatively small.

$$\begin{cases} z_{as} = z_a - l_s\varphi \\ z_{sf} = z_a - l_f\varphi \\ z_{sr} = z_a + l_r\varphi \end{cases} \tag{5}$$

where m_s is the vehicle seat mass, z_s is the seat's vertical displacement, m_a is the vehicle's sprung mass, z_a is the vertical displacement of the body centroid, F_s is the seat's suspension force, F_f and F_r are the forces of the front and rear suspensions, l_s is the horizontal distance from the seat to the centroid, l_f and l_r are the distances from the front and rear axles to the body centroid, φ is the body pitch angle, I_φ is the body pitch moment of inertia, k_f and c_f are the spring's stiffness and the damping coefficient of the front suspension, k_r and c_r are the spring's stiffness and the damping coefficient of the rear suspension, m_{uf} and m_{ur} are the front and rear unsprung mass, z_{uf} and z_{ur} are the vertical displacements of the front and rear unsprung mass, k_{tf} and k_{tr} are the equivalent stiffness of the front and rear tires, z_{rf} and z_{rr} are the displacement inputs of the front and rear wheels, z_{af} and z_{ar} are the vertical displacements of the front corner and rear corner of the vehicle's body. This study was carried out on the basis of a passenger car model in order to achieve an effective increase in ride comfort in passenger cars; the model for this study was built on a mature, commercially available model. Table 1 shows the parameters of the half vehicle model.

Table 1. Main parameters of the vehicle model.

Name	Value
Seat mass m_s (kg)	48
Body centroid mass m_a (kg)	928.2
Unsprung mass of front wheels m_{uf} (kg)	26.5
Unsprung mass of rear wheels m_{ur} (kg)	24.4
Distance from seat to centroid l_s (m)	0.324
Distance from front axle to centroid l_f (m)	0.968
Distance from rear axle to centroid l_r (m)	1.392
Moment of inertia aound the Y axis I_φ (kg·m^2)	1058
Front suspension stiffness k_f (kN·m^{-1})	25
Rear suspension stiffness k_r (kN·m^{-1})	22
Front suspension damping c_f (Ns/m)	1500
Rear suspension damping c_r (Ns/m)	1300
Tire stiffness k_t (kN·m^{-1})	192

3. Seat Suspension Layout

3.1. The Ball-Screw Mechatronic Inerter

The inerter is a mass element at both ends, and its output force is proportional to the relative acceleration at both ends. Inerters are available in ball-screw, rack and pinion, and fluid types. In this study, we have designed a ball-screw mechatronic inerter. The ball-screw mechatronic inerter comprises a rotary motor device and a ball-screw inerter. Among them, the ball-screw converts the linear reciprocating motion into a rotary motion and transmits it to the rotary motor. Figure 2 shows the working principle of the ball-screw mechatronic inerter.

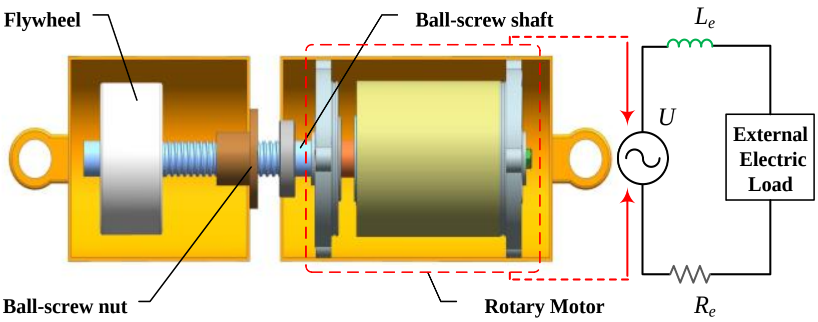

Figure 2. Ball-screw mechatronic inerter.

According to Figure 2, the inertance of the ball-screw mechatronic inerter can be changed by modifying the rotational inertia of the flywheel mounted on the ball-screw shaft. When both endpoints of the ball-screw mechatronic inerter move in a straight line, the rotating motor rotor is driven by the ball-screw shaft, producing a voltage U that flows through the external electrical load. R_e and L_e are the coil resistance and inductance. In this paper, the coil factor is not considered in the optimization. The external electrical load can be adopted to simulate the corresponding mechanical network in the optimization process.

3.2. The Seat Suspension Layout

The designed seat suspension, using the mechatronic inerter, includes a mechanical part and an electrical network part. For the mechanical section, we needed to provide load-bearing capacity for the seat suspension by means of a parallel spring, which includes a spring and an inerter, and provides a fundamental seat suspension layout to protect the system in the event of electrical network failure. The electrical section involves resistors, inductors, and capacitors to simulate the dampers, springs, and inerters. Figure 3 shows the layout of the mechatronic seat suspension, where the mechatronic inerter is connected, in parallel, with the spring.

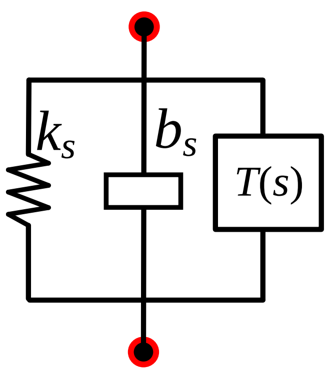

Figure 3. General layout of the seat suspension.

Where k_s and b_s are mechanical structures and $T(s)$ is the impedance expression to be solved; the double primary impedance transfer function is as follows:

$$T(s) = \frac{\alpha_1 s + \alpha_0}{\beta_1 s + \beta_0} \tag{6}$$

where $\alpha_i \geq 0$, $\beta_i \geq 0$ (β_i are not all 0). The positive real constraints of the double primary impedance transfer function are as follows:

$$\alpha_1 \beta_1 \geq 0 \tag{7}$$

The biquadratic impedance transfer function is as follows:

$$T(s) = \frac{\alpha_2 s^2 + \alpha_1 s + \alpha_0}{\beta_2 s^2 + \beta_1 s + \beta_0} \tag{8}$$

where $\alpha_i \geq 0$, $\beta_i \geq 0$ (β_i are not all 0). The positive realness constraints of the biquadratic impedance transfer function are as follows:

$$\left(\sqrt{\alpha_2 \beta_0} - \sqrt{\alpha_0 \beta_2}\right)^2 \leq \alpha_1 \beta_1 \tag{9}$$

The bicubic impedance transfer function is as follows:

$$T(s) = \frac{\alpha_3 s^3 + \alpha_2 s^2 + \alpha_1 s + \alpha_0}{\beta_3 s^3 + \beta_2 s^2 + \beta_3 s + \beta_0} \tag{10}$$

where $\alpha_i \geq 0$, $\beta_i \geq 0$ (β_i are not all 0). The positive realness constraints of the bicubic impedance transfer function are as follows:

$$\begin{cases} (\alpha_1 + \beta_1)(\alpha_2 + \beta_2) \geq (\alpha_0 + \beta_0)(\alpha_3 + \beta_3); \\ a_3 = 0, a_2 \geq 0, a_0 \geq 0, -a_1 \leq 2\sqrt{a_0 a_2}; \\ a_3 > 0, a_0 \geq 0, a_1 \geq 0, -a_2 \leq \sqrt{3a_1 a_3} or a_2^2 > 3a_1 a_3, 2a_2^3 - 9a_1 a_2 a_3 + 27a_0 a_3^2 \geq 2(a_2^2 - 3a_1 a_3)^{3/2} \end{cases} \tag{11}$$

where $a_0 = \alpha_0 \beta_0$, $a_1 = \alpha_1 \beta_1 - \alpha_0 \beta_2 - \alpha_2 \beta_0$, $a_2 = \alpha_2 \beta_2 - \alpha_1 \beta_3 - \alpha_3 \beta_1$, $a_3 = \alpha_3 \beta_3$.

4. Optimal Design of the Mechatronic Seat Suspension

For optimum performance of the mechatronic seat suspension, the parameters of the designed seat suspension systems are optimized via particle swarm optimization. To begin with, the particle is initialized, and the fit value of the particle is then compared with the best location it passes through, and the speed and position of the particle are updated. This ends when the termination condition is met. As the model for this study was built on a mature, commercially available model, before optimization, the main spring coefficient for protection remained the same as the conventional suspension, and only the parameters in $T(s)$ and b were optimized to give the optimization results practical significance.

Assuming the vehicle is driving at 30 km/h on a C grade road [29], and taking into account the vertical acceleration of the seat and the acceleration of the pitch motion; then, the objective function is defined as

$$f = \frac{J_1}{J_{1\text{pas}}} + \frac{J_2}{J_{2\text{pas}}} \tag{12}$$

where $J_{1\text{pas}}$ and $J_{2\text{pas}}$ are the root-mean-square (RMS) values of the seat vertical acceleration and the pitch motion acceleration of traditional passive suspension. Here, $J_{1\text{pas}}$ = 0.9913 m/s^2 and $J_{2\text{pas}}$ = 1.2852 rad/s^2. J_1 and J_2 are the RMS values of the seat vertical acceleration and the pitch motion acceleration of the designed suspension system. The mechanical inertance b and the $T(s)$ transfer function as the optimization variables. Particle swarm optimization was used to find the global optimum by following the current search. This algorithm has attracted academic attention for its ease of implementation, high accuracy and fast convergence. Equations (13) and (14) are the updated formulas for the particle velocity and position properties.

$$V^{n+1} = \lambda V^n + d_1 r_1 (P_{id}^n - X^n) + d_2 r_2 \left(P_{gd}^n - X^n\right) \tag{13}$$

$$X^{n+1} = X^n + V^{n+1} \tag{14}$$

where λ is the inertia factor, V is the velocity of the particle, X is the particle's position, n is the iterations number, and d_1 and d_2 are non-negative constants. The random numbers r_1 and r_2 usually have a value between 0 and 1, while P_{id} and P_{gd} are the individual extremum and global extremum. Figure 4 shows the optimization process of the algorithm.

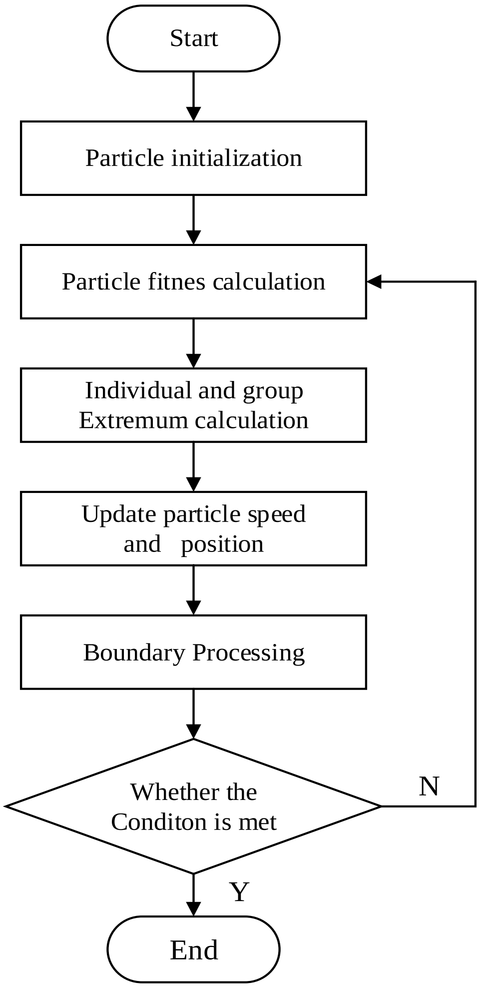

Figure 4. The optimization process of particle swarm optimization.

The optimized results of the transfer functions can be passively realized by the electrical network involving resistors, capacitors, and inductors. Figure 5 illustrates the corresponding network; Table 2 shows the detailed parameters.

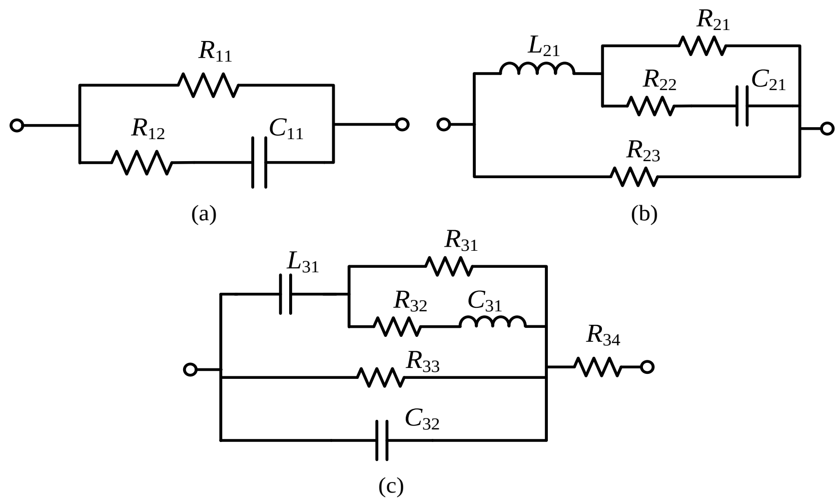

Figure 5. Electrical network. (**a**) Bivariate transfer function electrical network; (**b**) Biquadratic transfer function electrical network; (**c**) Bicubic transfer function electrical network.

Table 2. Electrical network parameters.

Name	Value
Resistor R_{11} (Ω)	4877
Resistor R_{12} (Ω)	654
Capacitor C_{11} (F)	0.0047
Resistor R_{21} (Ω)	98,754
Resistor R_{22} (Ω)	35,789
Resistor R_{23} (Ω)	5711
Capacitor C_{21} (F)	0.0079
Inductor L_{21} (H)	0.34
Resistor R_{31} (Ω)	81
Resistor R_{32} (Ω)	6998
Resistor R_{33} (Ω)	74,223
Resistor R_{34} (Ω)	158
Capacitor C_{31} (F)	0.0024
Capacitor C_{32} (F)	0.0017
Inductor L_{31} (H)	0.76

5. Performance Evaluation

The structural optimization of the designed seat suspension was required for the application of the mechatronic inerter. Table 3 shows the RMS values of the seat acceleration and pitch acceleration among the different suspension systems at a speed of 30 km/h.

Table 3. Comparison of the different seat suspension systems.

	RMS of Seat Acceleration	Improvement	RMS of Pitch Acceleration	Improvement
Passive suspension	0.9913	/	1.2852	/
Layout S1	0.9664	2.51%	1.2638	1.67%
Layout S2	0.9459	4.58%	1.2414	3.41%
Layout S3	0.8866	10.56%	1.1879	7.57%

Table 3 shows that, for the S1 seat suspension layout, the RMS values of the seat acceleration and the pitch acceleration decreased by 2.51% and 1.67%, respectively. The improvements are not obvious. Therefore, as the transfer function of the external electrical network increases in order, the RMS values of the seat acceleration and the pitch acceleration of the S2 seat suspension layout are further reduced by 4.58% and 3.41%, respectively. Then, for the S3 seat suspension layout, which used a bicubic transfer function electrical network, the RMS values of the seat acceleration and the pitch acceleration decreased by 10.56% and 7.57%, respectively; this resulted in a significant improvement in the ride comfort of the vehicle seat suspension. A comparison of the time domain characteristics of the seat acceleration and the pitch acceleration are shown in Figures 6 and 7. Figures 8 and 9 show the comparisons of the RMS values of the seat acceleration and the pitch acceleration at different speeds.

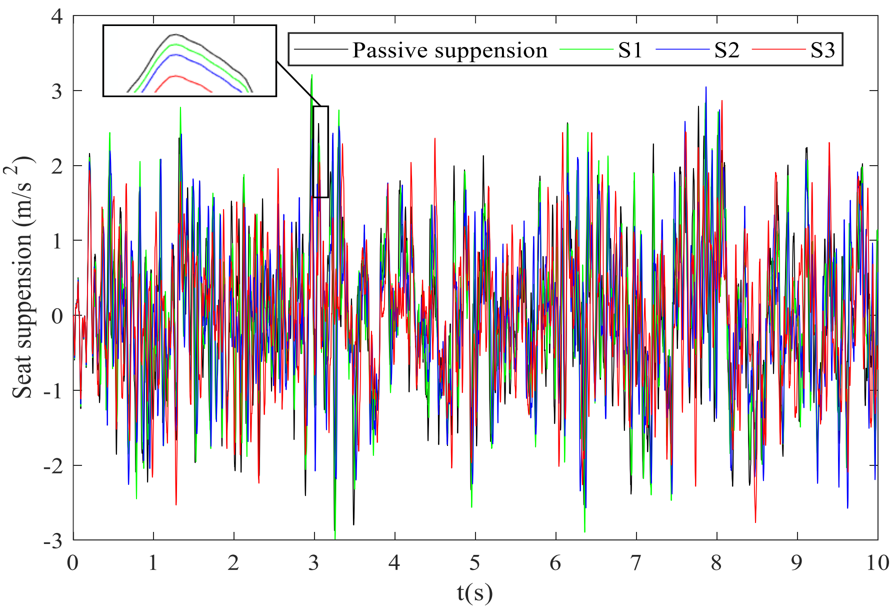

Figure 6. Comparison of the seat accelerations in the time domain.

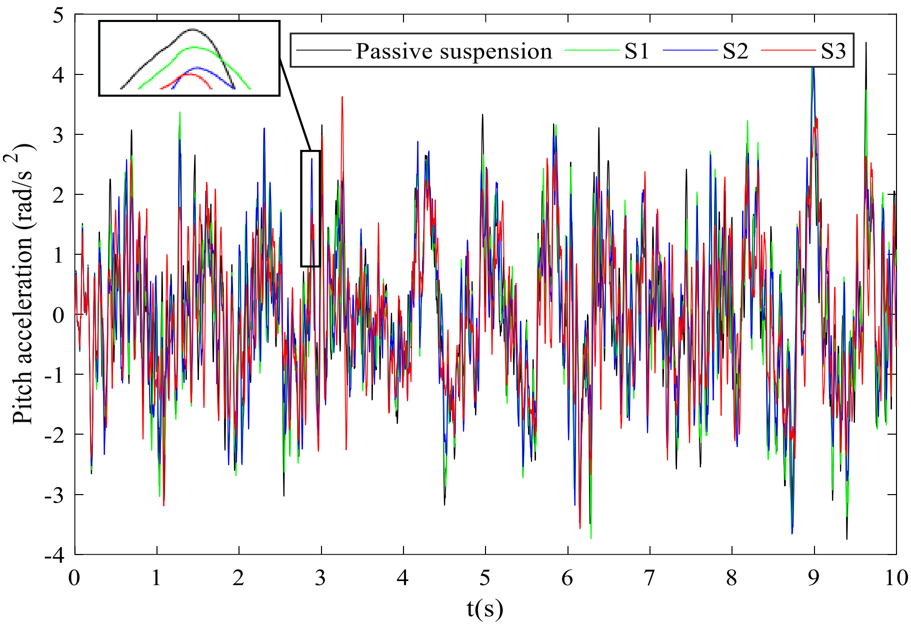

Figure 7. Comparison of the pitch accelerations in the time domain.

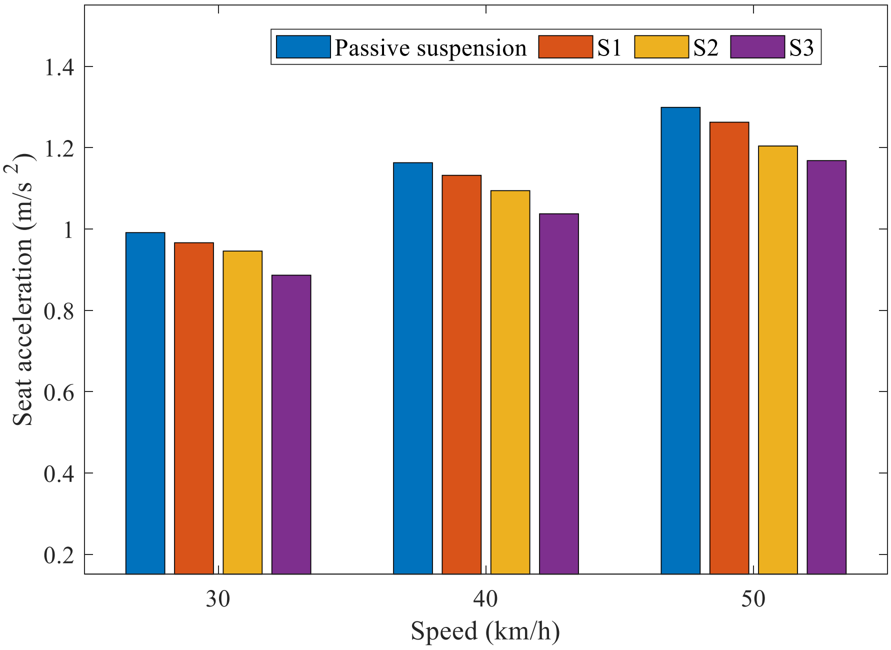

Figure 8. Comparison of the RMS of seat acceleration under different speeds.

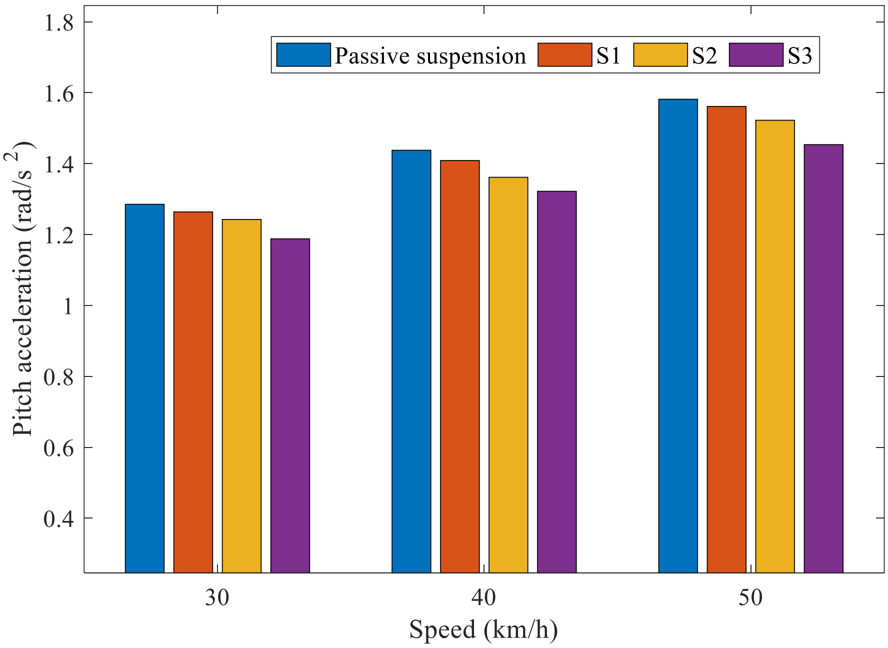

Figure 9. Comparison of the RMS of pitch acceleration under different speeds.

It is noted that, as the vehicle speed increases, the RMS values of the seat acceleration under the same suspension structure also increase. Under the same vehicle speed, the higher the transfer function order is, the smaller the RMS values of the seat acceleration are. For the pitch acceleration, as can be seen in the bar chart, when the speed of the vehicle increased, the pitch acceleration under the same type of suspension also increased. As the order of transfer function of the external electrical network increased, the pitch acceleration was reduced. In conclusion, the RMS values of the seat acceleration and pitch acceleration of the S3 layout are significantly lower than those of the S1 and S2 layouts, and passive suspension.

6. Conclusions

In this study, a mechatronic inerter element was introduced into the structural design of vehicle seat suspensions, and the problem of optimizing the design of the vehicle seat suspension, to integrate the mechatronic inerter element, was investigated. In addition, the vertical and pitch movements of the vehicle's sprung mass and the vertical vibration of the seat were considered in a half vehicle model. Based on a ball-screw mechatronic inerter, the external electrical networks, using different transfer function-orders, were optimized via the particle swarm optimization algorithm. The results show that, as the external electrical network transfer function-order is increased, the RMS values of the seat acceleration and pitch acceleration will be further reduced. The RMS values of the seat acceleration and pitch acceleration can be simultaneously reduced by 10.56% and 7.57%, respectively, at most. The performance of vehicle seat suspensions with an integrated mechatronic inerter element can be improved by increasing the order of the external electrical network transfer function.

Author Contributions: Conceptualization, C.Q.; methodology, Y.S.; software, X.L.; validation, X.L.; formal analysis, C.Q.; investigation, Y.S.; writing—original draft preparation, C.Q.; writing—review and editing, Y.S.; supervision, X.L. All authors have read and agreed to the published version of the manuscript.

Funding: This work was supported by the Natural Science Foundation of Beijing Municipality (No. 3214045), and the Natural Science Foundation of Jiangsu Province (No. BK20211364).

Data Availability Statement: The data used to support the findings of the study are available from the corresponding author upon request.

Conflicts of Interest: The authors declare no conflict of interest.

References

1. Choi, S.; Choi, Y.T.; Chang, E.G.; Han, S.J.; Kim, C.S. Control characteristics of a continuously variable ER damper. *Mechatronics* **1998**, *8*, 143–161. [CrossRef]
2. Rakheja, S.; Afework, Y.; Sankar, S. An analytical and experimental investigation of the driver-seat-suspension system. *Veh. Syst. Dyn.* **1994**, *23*, 501–524. [CrossRef]
3. Tong, R.T.; Amirouche, F. Ride control-a two state suspension design for cabs and seats. *Veh. Syst. Dyn.* **1999**, *33*, 578–589. [CrossRef]
4. Wereley, N.M.; Pang, L. Nondimensional analysis of semi-active electrorheological and magnetorheological dampers using approximate parallel plate models. *Smart Mater. Struct.* **1997**, *7*, 732–743. [CrossRef]
5. Amirouche, F.; Palkovics, L.; Woodrooffe, J. Optimal driver seat suspension design for heavy trucks. *Transp. Syst. ASME* **1994**, *2*, 277–291.
6. Andersson, R. The low back pain of bus drivers in an urban area of California. *Spine* **1982**, *17*, 1481–1488. [CrossRef]
7. Deng, H.; Deng, J.; Yue, R.; Han, G.; Zhang, J.; Ma, M.; Zhong, X. Design and verification of a seat suspension with variable stiffness and damping. *Smart Mater. Struct.* **2019**, *28*, 65015. [CrossRef]
8. Ning, D.; Du, H.; Sun, S.; Li, W.; Zhang, N.; Dong, M. A novel electrical variable stiffness device for vehicle seat suspension control with mismatched disturbance compensation. *IEEE ASME Trans. Mechatron.* **2019**, *24*, 2019–2030. [CrossRef]
9. Liao, X.; Du, X.; Li, S. Design of cab seat suspension system for construction machinery based on negative stiffness structure. *Adv. Mech. Eng.* **2021**, *13*, 1–15. [CrossRef]
10. Liu, P.; Ning, D.; Luo, L.; Zhang, N.; Du, H. An electromagnetic variable inertance and damping seat suspension with controllable circuits. *IEEE Trans. Ind. Electron.* **2021**, *69*, 2811–2821. [CrossRef]
11. Smith, M.C.; Wang, F. Performance benefits in passive vehicle suspensions employing inerters. *Veh. Syst. Dyn.* **2004**, *42*, 235–257. [CrossRef]
12. Zhang, C.; Zhang, Z.; Zhao, H. Analysis of dynamic characteristics and ride performance of automobile active suspension. *Chin. Agric. Mech.* **2015**, *36*, 176–179. [CrossRef]
13. Huang, C.; Chen, L.; Yuan, Z.; Jiang, H.; Niu, L. Hybrid fuzzy control of semi-active suspension system. *Automot. Eng.* **2014**, *36*, 999–1018.
14. Smith Malcolm, C. Synthesis of mechanical networks: The inerter. *IEEE Trans. Autom. Control* **2002**, *47*, 1648–1662. [CrossRef]
15. Zhao, Z.-P.; Chen, Q.-J.; Zhang, R.-F.; Pan, P.; Jian, Y.-Y. Energy dissipation mechanism of inerter systems. *Int. J. Mech. Sci.* **2020**, *184*, 105845. [CrossRef]
16. Chen, M.Z.Q.; Hu, Y.L.; Li, C.Y.; Chen, G. Application of semi-active inerter in semi-active suspensions via force tracking. *J. Vib. Acoust.* **2016**, *138*, 041014. [CrossRef]

17. Hu, Y.L.; Wang, K.; Chen, Y.H.; Chen, M.Z.Q. Inerter-based semi-active suspensions with low-order mechanical admittance via network synthesis. *Trans. Inst. Meas. Control* **2018**, *40*, 4233–4245. [CrossRef]
18. Liu, Y.L.; Zhao, W.T.; Yang, X.F.; Shen, Y.J. Predictive control of vehicle ISD suspension based on a hydraulic electric inerter. *Shock Vib.* **2019**, *2019*, 9230736. [CrossRef]
19. Zhang, S.Y.; Jiang, J.Z.; Neild, S.A. Optimal configurations for a linear vibration suppression device in a multi-storey building. *Struct. Control Health Monit.* **2016**, *24*, e1887. [CrossRef]
20. Giaralis, A.; Petrini, F. Wind-induced vibration mitigation in tall buildings using the tuned mass-damper-inerter. *J. Struct. Eng.* **2017**, *142*, 04017127. [CrossRef]
21. Yang, L.; Wang, R.; Ding, R.; Liu, W.; Zhu, Z. Investigation on the dynamic performance of a new semi-active hydro-pneumatic inerter-based suspension system with MPC control strategy. *Mech. Syst. Signal Process.* **2021**, *154*, 107569. [CrossRef]
22. Shen, Y.; Hua, J.; Fan, W.; Liu, Y.; Yang, X.; Chen, L. Optimal design and dynamic performance analysis of a fractional-order electrical network-based vehicle mechatronic ISD suspension. *Mech. Syst. Signal Process.* **2023**, *184*, 109718. [CrossRef]
23. Li, Y.; Yang, X.; Shen, Y.; Liu, Y.; Wang, W. Optimal design and dynamic control of the HMDV inertial suspension based on the ground-hook positive real network. *Adv. Eng. Softw.* **2022**, *171*, 103171. [CrossRef]
24. Shen, Y.; Chen, L.; Liu, Y.; Zhang, X. Influence of fluid inerter nonlinearities on vehicle suspension performance. *Adv. Mech. Eng.* **2017**, *9*, 1687814017737257. [CrossRef]
25. Sun, X.Q.; Chen, L.; Wang, S.H.; Zhang, X.L.; Yang, X.F. Performance investigation of vehicle suspension system with nonlinear ball-screw inerter. *Int. J. Automot. Technol.* **2016**, *17*, 399–408. [CrossRef]
26. Liu, C.; Chen, L.; Zhang, X.; Yang, Y.; Nie, J. Design and tests of a controllable inerter with fluid-air mixture condition. *IEEE Access* **2020**, *8*, 125620–125629. [CrossRef]
27. Yang, X.; He, T.; Shen, Y.; Liu, Y.; Yan, L. Research on predictive coordinated control of ride comfort and road friendliness for heavy vehicle ISD suspension based on the hybrid-hook damping strategy. *Proc. Inst. Mech. Eng. D J. Automob. Eng.* **2022**. [CrossRef]
28. Shen, Y.; Hua, J.; Wu, B.; Chen, Z.; Xiong, X.; Chen, L. Optimal design of the vehicle mechatronic ISD suspension system using the structure-immittance approach. *Proc. Inst. Mech. Eng. D J. Automob. Eng.* **2022**, *236*, 512–521. [CrossRef]
29. *ISO 8608:2016*; Mechanical Vibration—Road Surface Profiles—Reporting of Measured Data. International Organization for Standardization: Geneva, Switzerland, 2016. Available online: https://www.iso.org/standard/71202.html. (accessed on 22 November 2022).